Bull. Chem. Soc. Ethiop. **2021**, 35(3), 601-614.
DOI: https://dx.doi.org/10.4314/bcse.v35i3.11

ISSN 1011-3924
Printed in Ethiopia
Online ISSN 1726-801X

EXPERIMENTAL AND THEORETICAL INVESTIGATIONS (FTIR, UV-VIS SPECTROSCOPY, HOMO-LUMO, NLO AND MEP ANALYSIS) OF AMINOTHIOPHENOL ISOMERS

Taner Kalaycı[1], Neslihan Kaya Kınaytürk[2*] and Belgin Tunalı[2]

[1]Bandırma Onyedi Eylül University, Vocational School of Health Services, Bandırma, Balıkesir, Turkey
[2]Burdur Mehmet Akif Ersoy University, Faculty of Arts and Sciences, Department of Nanoscience and Nanotechnology, Burdur, Turkey

(Received November 29, 2021; Revised January 4, 2022; Accepted January 10, 2022)

ABSTRACT. In this research, theoretical and experimental investigation was performed on the structural and spectral data of aminothiophenol isomers. The theoretical electronic structure analyses were performed by density functional theory at the B3LYP level with the LanL2DZ basis set in the gas phase of the isolated compounds at the ground state. Potential energy distribution analysis was performed to determine the assignments of the vibration bands. Experimental and theoretical spectroscopic data were compared. Energy gap, ionization potential, electron affinity, and electronegativity were obtained through frontier molecular orbitals.

KEY WORDS: Aminothiophenols, Density functional theory, Polarizability, Vibrational assignments, Molecular electrostatic potential surface

INTRODUCTION

Aminothiophenol (ATP) isomers (mercaptoanilines, aminobenzenthiols) are organic compounds with a ring structure to which a-SH and a-NH_2 functional groups are attached to the benzene ring. Aromatic thiols have interesting properties with ortho, meta and para positions and they have been the subject of many studies for years [1–6]. Batz *et al.* investigated a study on the electrochemical properties of ATP isomers adsorbed on gold and mentioned that most of the functionalized thiophenol isomers can be used for surface modification by undergoing electrochemical transformations [7]. In the literature search, it has been seen that ATP derivatives are frequently used in corrosion prevention processes because they contain single electron pairs such as thiol and amine groups in the benzene ring [8, 9]. In the paper of Li *et al.*, they used molecular dynamics simulation to investigate the inhibitory adsorption of four thiophenol derivatives on the surface of Fe (001) in 0.1 M hydrochloric acid solution. They wrote that the corrosion inhibition performance mainly depends on the interaction between polar groups and metal surface [10]. Kabel *et al.* investigated the inhibition efficiency for corrosion due to its 2-ATP adsorbing property [1].

Similar studies have been reported by Karthik *et al.* and Anto Maria Jeraldin *et al.* [11, 12]. The synthesis and antibacterial properties of poly (ATPs) were reported by Anto Maria *et al.* and Sorasaenee *et al.* in other studies [13, 14].

There have been studies showing significant changes in the relative SERS (surface-enhanced Raman spectroscopy) intensities when ATP isomers were used as a probe molecule and adsorbed on some metals [15–17]. Sun et al. used the 4-ATP + Ag complex to visualize the chemical mechanism between the 4-ATP and metal complexes [18]. Jiang *et al.* reported photo-induced surface catalytic binding reactions of ATPs by SERS and density functional theory (DFT) methods [19]. In the literature, adsorption of 4-ATP on Au was performed and geometric and electronic structure was investigated by using DFT [6, 20].

*Corresponding author. E-mail: nkinayturk@mehmetakif.edu.tr

As it can be seen from the research in the literature, while several experimental and theoretical studies for ATPs have been ascertained, no study has been searched examining the structural change of the isomer and its effect on the characterization of the compounds in detail. In this study, it was aimed to investigate structural differences in the molecule caused by the position of the amine and thiol group in the phenyl ring by experimental and theoretical spectroscopic analyses.

DFT is a powerful method for revealing the geometric differences of isomers precisely and allows an estimate to be made before designing new experiments. In this study, molecular geometry, vibration spectra and assignments, HOMO-LUMO energies, Mulliken charges and polarizability were determined, and experimental results were compared with theoretical results. We anticipate that the identification of the characteristic structural differences of isomers will make an important contribution to the literature.

EXPERIMENTAL

ATPs were obtained commercially, from Aldrich (2-ATP and 3-ATP) and Merck (4-ATP) company. They are all analytical grade purity. The spectroscopic measurements were recorded at room temperature. FTIR spectroscopic analyses were carried out by Perkin Elmer Spectrum BX model. UV-Vis analyses were performed by Shimadzu 1280 Spectrophotometer.

Quantum chemical calculations were performed by using the DFT method with the B3LYP function and LanL2DZ basis set. Gaussian 09 [21] software package was used for the theoretical calculations. The geometry optimizations were followed by frequency calculations using the same basis set. Time-dependent DFT (TD-DFT) method was used to obtain UV-Vis Spectra and electronic properties. The results were visualized using the Gauss View and Chemcraft 1.8 program [22]. Potential energy distribution, corresponding to the observed frequencies, was calculated using VEDA program [23].

RESULTS AND DISCUSSION

Molecular geometry

The molecular crystal structures of the title compounds are shown in Figure 1a, b, c. The numerical values of the bond lengths are written on Figure 1. The calculated bond angles of all molecules are summarized in Table 1.

The bond length of the C1 atom with the C2 and C6 atoms is the same in all isomers and its value is 1.42 Å. Again, in ATPs, the bond length of the C1 atom with the N1 atom is the same and its value is 1.39 Å. When all bond lengths are examined, the highest bond length is detected where the carbon atom is attached to the sulfur atom.

In Figure 1, these conjunction points are C2-S1, C3-S1 and C4-S1, they have the value of 1.86, 1.85 and 1.86 Å, respectively. The shortest bond length is observed between the nitrogen atom and the hydrogen atom with the value of 1.01 Å for each isomer.

When the bond angles are examined, it is determined that the smallest bond angle is between C-S-H atoms with a value of around 97° among all isomers in Table 1. The bond angle between C2-C1-C6 is important in terms of showing the place where NH_2 is attached to the ring from the C1 atom. By investigating this bond, it is observed that there is a slight decrease in bond angle for 2-ATP, 3-ATP, and 4-ATP, respectively. The fact that the SH group gradually moves away from the NH_2 group may be the reason for this decrease in the bond angle.

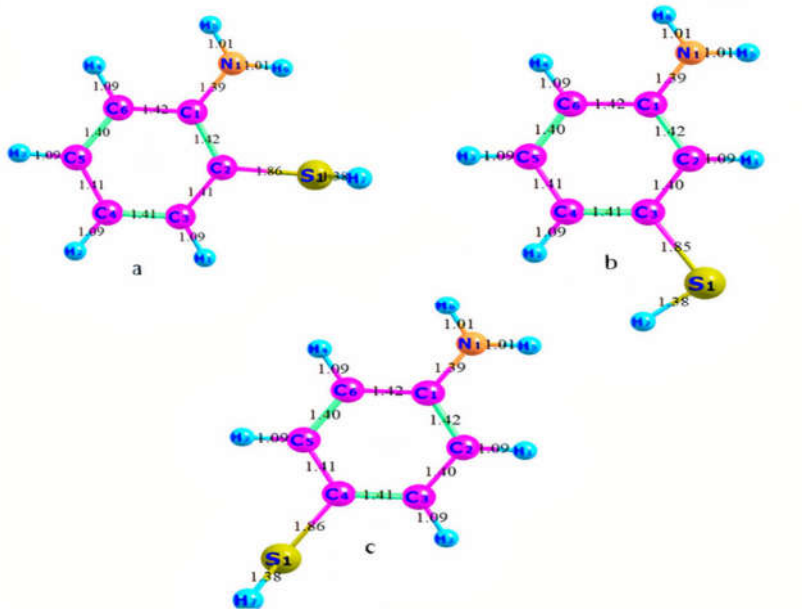

Figure 1. Geometric structure of (a) 2-ATP, (b) 3-ATP and (c) 4-ATP.

Table 1. Optimized parameters for 2-ATP, 3-ATP and 4-ATP (bond angles) (°: degree).

2-ATP		3-ATP		4-ATP	
Atoms	bond angles [°]	Atoms	bond angles [°]	Atoms	bond angles [°]
C2-C1-C6	119.3	C2-C1-C6	119.1	C2-C1-C6	118.6
C2-C1-N1	121.5	C2-C1-N1	120.3	C2-C1-N1	120.7
C6-C1-N1	120.5	C6-C1-N1	120.6	C6-C1-N1	120.7
C1-C2-C3	120.6	C1-C2-C3	120.1	C1-C2-C3	120.5
C1-C2-S1	120.0	C1-C2-H1	119.5	C1-C2-H1	119.8
C3-C2-S1	122.6	C3-C2-H1	120.3	C3-C2-H1	119.8
C2-C3-H1	119.3	C2-C3-C4	121.0	C2-C3-C4	120.7
C2-C3-C4	119.0	C2-C3-S1	116.8	C2-C3-H2	119.7
C4-C3-H1	120.3	C4-C3-S1	122.2	C4-C3-H2	119.6
C3-C4-C5	118.9	C3-C4-C5	118.5	C3-C4-C5	119.9
C3-C4-H2	120.3	C3-C4-H2	121.8	C3-C4-S1	120.4
C5-C4-H2	120.8	C5-C4-H2	120.2	C5-C4-S1	120.4
C4-C5-C6	120.8	C4-C5-C6	121.4	C4-C5-C6	120.6
C4-C5-H3	119.9	C4-C5-H3	119.2	C4-C5-H3	119.6
C6-C5-H3	119.3	C6-C5-H3	119.4	C6-C5-H3	119.8
C1-C6-C5	120.9	C1-C6-C5	119.8	C1-C6-C5	120.5
C1-C6-H4	119.0	C1-C6-H4	119.9	C1-C6-H4	119.8
C5-C6-H4	120.1	C5-C6-H4	120.3	C5-C6-H4	119.8
C1-N1-H6	119.6	C1-N1-H5	121.0	C1-N1-H5	120.9
C1-N1-H5	120.6	C1-N1-H6	120.8	C1-N1-H6	120.9
H5-N1-H6	119.2	H5-N1-H6	118.2	H5-N1-H6	118.2
C2-S1-H7	97.6	C3-S1-H7	97.1	C4-S1-H7	97.7

IR spectroscopic analysis

ATR device is used for ATP isomers with the range between 4000-600 cm^{-1}. Experimental and Theoretical IR spectra for 2-ATP, 3-ATP and 4-ATP are shown in Figure 2 and Figure 3, respectively. The IR and Raman bands positions calculated with the method B3LYP/ LanL2DZ and their assignments are reported in Table 2. The main objective of this study is to investigate the results of intermolecular interactions occurring in ATP isomers. Isomer effects have been studied through some vibrational bands. For this purpose, characteristic vibration bands were examined in detail and the compatibility of experimental and theoretical results was observed.

The band characteristics of the NH groups are usually observed around 3500-3300 cm^{-1} [1, 2]. While the N-H bands for 2-ATP were experimentally observed at 3438 and 3349 cm^{-1} in the IR spectrum they were calculated as 3617 and 3473 cm^{-1} theoretically [24]. Similarly, these bands for 3-ATP were observed at 3427 and 3348 cm^{-1}, while they were calculated at 3632 and 3497 cm^{-1}. For 4-ATP, it was observed at 3427 and 3348 cm^{-1} and calculated at 3630 and 3496 cm^{-1}.

In the FT-IR spectrum, the S-H stretching vibration band is observed around 2530 cm^{-1} [2, 25, 26]. This band was calculated for 2-ATP, 3-ATP, and 4-ATP at 2363, 2427, 2364 cm^{-1}, respectively, and it was observed experimentally at 2522, 2553 and 2545 cm^{-1}, respectively. Correspondingly, in the Raman spectroscopic resources, these vibrations appear at 2532 cm^{-1} for 2-ATP and 2544 cm^{-1} for 4-ATP cm^{-1} [5, 27].

For aromatic and heteroatomic structures, C-H stretching vibrations usually appear in the range of 3200-3000 cm^{-1} [5, 19, 28]. These modes are not affected by subgroups and are therefore pure vibration modes. Asymmetric and symmetrical C-H stretching vibrations are observed in the FT-IR spectrum of the 2-ATP, at 3061 and 3016 cm^{-1} [24]. The corresponding bands are observed in the range 3075 and 3057 cm^{-1} in the calculated form. In the FT-IR spectrum of 3-ATP, asymmetric C-H stretching vibration is observed at 3048 cm^{-1} [24] and this band is calculated at 3065 cm^{-1}. Symmetrical C-H stretching vibration is observed at 3024 cm^{-1} for 4-ATP. The corresponding bands are calculated in near 3060 cm^{-1} [2, 19, 24]. The 900-675 cm^{-1} range is the region with the most informative bands in the spectra of aromatic compounds [29] and this region is inside in the 1500-600 cm^{-1} range known as fingerprints [30]. The C-H in-plane bending vibrations appear at 1480 cm^{-1}, 1327 cm^{-1}, 1275 cm^{-1} and 1144 cm^{-1} for 2-ATP and 1483 cm^{-1},

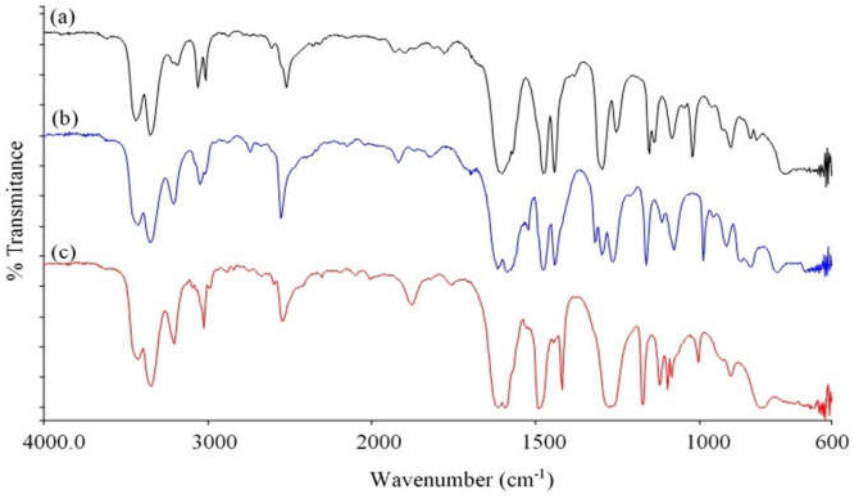

Figure 2. The experimental infrared spectra of ATP isomers (a) 2-ATP, (b) 3-ATP and (c) 4-ATP.

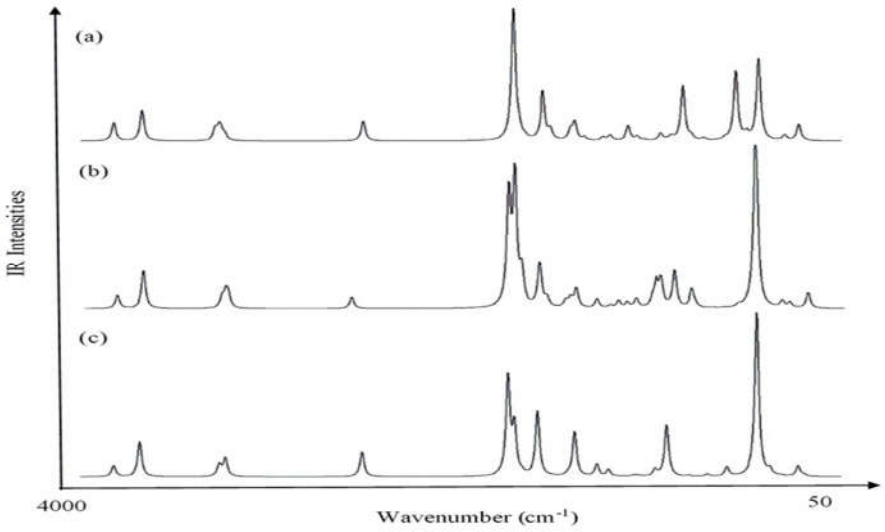

Figure 3. The theoretical infrared spectra of ATP isomers (a) 2-ATP, (b) 3-ATP and (c) 4-ATP.

Table 2. Detailed assignments of experimental and theoretical wavenumbers (cm^{-1}) of 2-ATP, 3-ATP and 4-ATP, along with potential energy distribution (PED).

Theoretical		Experimental			Theoretical		Experimental			Theoretical		Experimental		
2-ATP	Scaled	IR	Raman [2, 20 ,21,33]	Assignment (%PED)	3-ATP	Scaled	IR	Raman [6, 20-22, 33]	Assignment (%PED)	4- ATP	Scaled	IR	Raman [6, 12, 16, 20, 22 ,33]	Assignment (%PED)
3768	3617	3438s		ν_{NH} (98)	3783	3632	3427s		ν_{NH} (100)	3781	3630	3427s		ν_{NH} (100)
3618	3473	3349vs		ν_{NH} (98)	3643	3497	3348vs		ν_{NH} (100)	3642	3496	3348s		ν_{NH} (100)
3235	3106			ν_{CH} (94)	3223	3094	3210m		ν_{CH} (96)	3225	3096	3207m		ν_{NH} (99)
3214	3085			ν_{CH} (97)	3203	3075		3081s	ν_{CH} (90)	3220	3091			ν_{CH} (99)
3203	3075	3061m	3068vs	ν_{CH} (100)	3193	3065	3048m	3053vs	ν_{CH} (99)	3190	3062			ν_{CH} (100)
3184	3057	3016m	3047vs	ν_{CH} (96)	3186	3059		3044s	ν_{CH} (99)	3187	3060	3024m	3048s	ν_{CH} (99)
2461	2363	2522m	2532s	ν_{SH} (100)	2528	2427	2553m		ν_{SH} 100	2462	2364	2545m	2544s	ν_{SH} (100)
1673	1673			δ_{HNH} (78)	1688	1688		1701m	δ_{HNH} (95)	1688	1688			δ_{HNH} (94)
1645	1645	1603b	1610m	ν_{CC} (46)+δ_{HNH} (14)+ δ_{HCC} (13)	1656	1656	1630m	1638b	ν_{CC} (53)+ δ_{HCC} 10	1655	1655	1614b		ν_{CC} (44) + δ_{HCC} 16
1613	1613	1573sh	1586s	ν_{CC}(59)+δ_{CCC}(11)	1619	1619	1599b	1618m	ν_{CC} (64)+δ_{CCC}(28)	1615	1615	1595b	1593s	ν_{CC} (59) + δ_{CCC} 26
1520	1520	1477s	1476w	ν_{NC}(16)+ δ_{HCC} (37) + δ_{CCC} (18)	1522	1522	1520w	1498m	ν_{NC}(10)+ ν_{CC} (14)+ δ_{HCC} (32)+ δ_{CCC}(11)	1531	1531	1491s	148m	δ_{HCC} (48)+ ν_{CC} (16) + ν_{NC} (11)+ δ_{CCC} (10)
1480	1480	1445s		ν_{NC} (23)+δ_{HCC}(45)	1483	1483	1477s	1476w	ν_{CC}(26)+δ_{HCC} (21)	1456	1456	1446m		ν_{CC} (45)+ δ_{HCC} (35)

1376	1348			ν_{CC} (82)	1381	1353		1389w	ν_{CC}(80)+δ_{HCC} (11)	1374	1347			ν_{CC} (73) + δ_{HCC} (13)
1354	1327	1299s	1307m	ν_{NC} (27)+δ_{HCC}(42)	1355	1328	1300m	1370vw	ν_{NC}(13)+ δ_{HCC}(60)	1334	1307			δ_{HCC}(48) + ν_{NC}(25)+ν_{CC}(25)
1301	1275	1257m	1260m	δ_{HCC}(45)+ν_{CC}(10)+ν_{NC}(12)	1325	1299	1267s	1266w	δ_{HCC} (44)+ν_{NC}(31)	1333	1306	1274b	1261w	δ_{HCC}(47)+ ν_{NC}(25)+ν_{CC}(24)
1204	1180	1157m	1160m	δ_{HCC}(79)	1213	1189	1165m	1170w	δ_{HCC}(72)	1218	1194	1175s		ν_{HCC}(79)+ ν_{CC}(17)
1167	1144	1140m		ν_{CC} (27)+ δ_{HCC} (45)	1144	1121		1106m	ν_{CC} (33)+ δ_{HCC} (40) + δ_{HNC}(11)	1154	1131		114m	δ_{HCC} (56)+ ν_{CC}(18)+ δ_{HNC}(10)
1072	1051	1055m		ν_{CC}(21)+ ν_{SC}(11)+ δ_{HNC}(36)	1100	1078		1071s	δ_{HCC}(28) + ν_{CC}(34)	1107	1085	1080m	1087s	ν_{CC}(52)+ν_{SC}(16)+ δ_{HCC}(17)
1065	1044		1028vs	ν_{CC} (21)+ δ_{HCC}(26)+ δ_{CCC}(21)	1051	1030			ν_{CC}(15) + δ_{HNC} (62)	1041	1020			δ_{HNC}(65)+ ν_{CC}(16)
1025	1005			ν_{CC}(29)+ δ_{HNC}(24)+ δ_{CCC}(28)	1003	983	980w		ν_{CC}(32)+ δ_{CCC} (57)	1020	1000	100w	100m	δ_{CCC}(75)
1019	999	993m		τ_{HCCC}(52)+ τ_{CCCC}(30)	1002	982			τ_{HCCC} (77)+τ_{CCCC} (17)	1001	981			τ_{CCCC}(81)
987	967			τ_{HCCC}(80)	918	900	900m		δ_{HSC} (56)	991	971			τ_{HCCC}(53)+ τ_{CCCC}(27)
904	886		914w	δ_{HSC}(63)+ τ_{HCCC}(14)	897	879			τ_{HCCC}(69)+ τ_{NCCC}(15)	907	889		880m	δ_{HSC}(70)+ τ_{HCCC}(11)
876	858	849m		τ_{HCCC}(61)+ δ_{HSC}(23)	889	871	860w		τ_{HCCC}(81)	848	831		818m	τ_{HCCC}(49)+ δ_{HSC}(17)+ γ_{NCCC}(21)
847	830	829w	837s	δ_{CCC}(37)+ν_{NC}(20)+ ν_{CC}(13)	871	854	845w		ν_{NC}(13)+δ_{HSC}(36)+ δ_{CCC}(10)					
786	770	744w		τ_{NCCC}(14)+ γ_{HCCC}(61)	799	783			τ_{HCCC}(55)+ τ_{CCCC}(15)	833	816	813w		ν_{NC}(19)+ν_{CC}(32)+ δ_{CCC}(36)
743	728			τ_{HCCC}(36)+ τ_{CCCC}(32)+ γ_{NCCC}(10)	707	693			τ_{HCCC}(44)+ τ_{CCCC}(34)	730	715			τ_{CCCC}(42)+ τ_{HCCC}(30)
677	663		680s	ν_{SC}(14)+ δ_{CCC}(76)	688	674			ν_{SC}(12)+ δ_{CCC} (62)	653	640			δ(CCC) 75
565	554			δ(CCC)37	594	582			τ_{HCCC}(11)+ τ_{CCCC}(14)+ γ_{NCCC}(40)+ γ_{SCCC} (27)	632	619			ν_{SC}(33)+ δ_{CCC}(29)+ ν_{NC}(10)
562	551			τ_{HCCC}(14)+ τ_{CCCC}(16)+ γ_{NCCC}(20)	541	530			ν_{NC}(11)+ δ_{CCC} (58)	526	515		508vw	γ_{NCCC}(42)+ τ_{CCCC}(18)+τ_{HCCC} (29)
510	500			τ_{HNCC}(76)	455	446			τ_{CCCC}(47)+ τ_{HCCC}(19)+ γ_{SCCC}(14)+ γ_{NCCC}(11)	431	422			τ_{CCCC}(77)+ τ_{HCCN}(16)
460	451		475m	ν_{SC}(19)+ δ_{CCC} (15)+ δ_{NCC}(50)	412	404			δ_{NCC}(56)	399	391			δ_{NCC} (65)+ δ_{SCC}(13)

(ν = stretching; δ = deformation bending; τ = torsion; γ = in plane bending; vs = very strong; s = strong; m = medium; w = weak; vw = very weak; b = broad; sh = shoulder).

1328, 1299 and 1121 cm^{-1} for 3-ATP. On the other hand, the C-H in-plane bending vibrations appear at 1456, 1307, 1306 and 1131 cm^{-1} for 4-ATP. In addition to, the C-H out-of-plane bending vibrations appear at 999, 967 and 770 cm^{-1} for 2-ATP; 982, 879, 871 and 783 cm^{-1} for 3-ATP; 971, 889, 831, 715 cm^{-1} for 4-ATP. These results line up with the experimental ones [31, 32]. According to the PED results, these in-plane and out-of-plane bending vibrations are mixed modes mostly combined with other bending and stretching modes.

Vibration bands observed in the range of 1650–1430 cm^{-1} are attributed to aromatic C-C vibrations [24, 34, 35]. While these bands were observed experimentally in the range of 1603-1477 cm^{-1}, they were calculated in the range of 1645-1348 cm^{-1} for 2-ATP. In addition, the band observed in the experimental spectra at 1630 cm^{-1} was assigned as the C-C vibrational band in the range of 1656-1353 cm^{-1} in the spectrum calculated for 3-ATP. In experimental data, bands at 1614 cm^{-1} and 1595 cm^{-1} are assigned as C-C vibrations calculated in the range of 1655-1347 cm^{-1} for 4-ATP [2, 5, 19]. These vibration modes are highly mixed modes with an additive range of 82-44% and are often combined with HNC, HCC and HNH vibrations as well as some bending vibrations. For ATP isomers, these differences can be said to be caused by both the change in where the amine group is attached to the phenyl ring and the distance between the amine and thiol group.

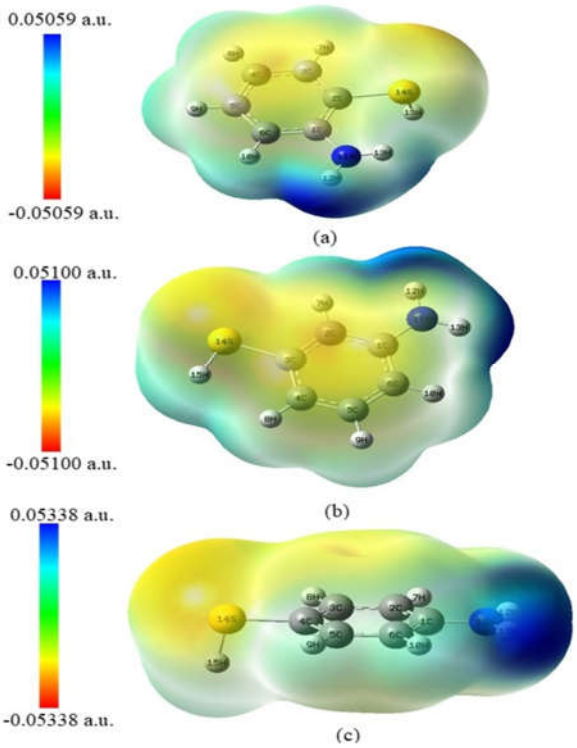

Figure 4. Molecular electrostatic potential map of (a) 2-ATP, (b) 3-ATP and (c) 4-ATP.

Molecular electrostatic potential surface analysis

The molecular electrostatic potential surface (MEP) maps present the charge distribution of the molecules and enable us to observe a variable charge region. Figure 4 shows the MEP surfaces of the ATP isomers a ranging from darkest red to deepest blue. The blue color indicates nucleophilicity, the red color indicates electrophilicity and the green color indicates the neutral, zero electrostatic potential region, which refers to hydrogen-bond interactions [36, 37]. The surface maps of MEP show that regions with negative potential are on sulfur, nitrogen and carbon atoms, and regions with positive potential are on hydrogen atoms attached to the amine group. When the MEP surface maps are examined, it is observed that the negative and positive charge densities of 4-ATP are concentrated at the opposite ends of the molecule. Therefore, we can say that the 4-ATP molecule has bigger polarizability than others and the results of NLO analysis also support this idea.

HOMO and LUMO analyses and chemical activity

In frontier molecular orbitals, HOMO denotes a wide variety of donor orbitals, while LUMO denotes acceptor orbitals. HOMO is the highest occupied energy orbital that can function as an electron donor. The LUMO is the lowest unoccupied energy orbital, which has enough space to accept electrons and can act as an electron acceptor [38]. HOMO-LUMO values give information about the polarization, electronegativity, hardness, reactivity, and kinetic stability of the molecule. [39, 40]. Surface images are shown in Figure 5, the most likely spectral parameters corresponding to wavelengths and electronic transitions are presented Table 3, and chemical reactivity indices are presented in Table 4.

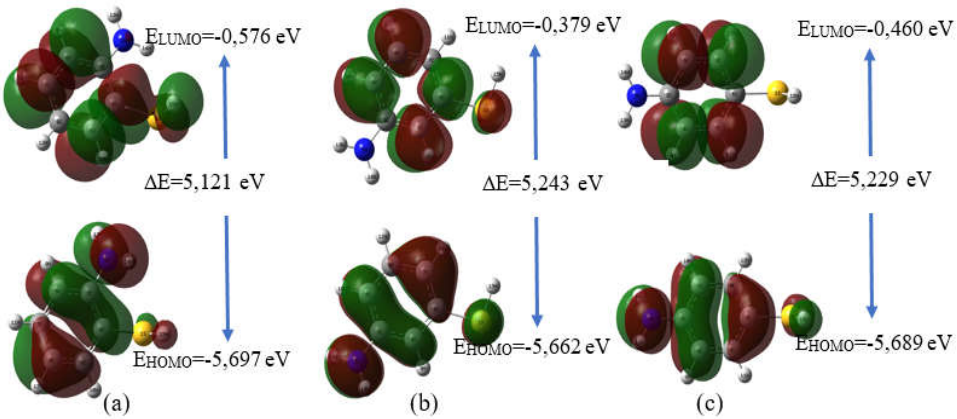

Figure 5. HOMO and LUMO plot of (a) 2-ATP, (b) 3-ATP and (c) 4-ATP.

The data obtained from the results show that ATPs have high hardness and low softness parameters due to their high energy gaps. These indicate that these molecules have low chemical activity, high kinetic stability, and it can therefore be concluded that they are highly stable. The results of chemical reactivity descriptors indicate higher hardness and lower softness values, lower intermolecular charge transfer and thus lower polarity.

Table 3. The experimental and calculated UV-Vis excitation energies and oscillator strength (f) for 2- ATP, 3- ATP, 4- ATP.

Molecule	C1 expansion coefficient	Excitation energy [eV]	λ_{exp} [nm]	λ_{cal} [nm]	f Oscillator strengths	Major contributions
2-ATP		4,4479	265	278,75	0,0848	
	0.68249					HOMO→LUMO (93%)
		5.4350		228	0.1463	
	0.63603					HOMO→LUMO+1 (80%)
		5.5556	210	223	0.0189	
	0.45314					HOMO-2→LUMO (41%)
	0.51269					HOMO-1→LUMO (52%)
3-ATP		4.5201	260	274.29	0.0642	
	0.66489					HOMO→LUMO (88%)
		5.3407	220	232.15	0.0002	
	0.67925					HOMO→LUMO+2 (92%)
		5.3651		231.10	0.0434	
	0.51361					HOMO-1→LUMO (53%)
	-0.48232					HOMO→LUMO (47%)
4-ATP		4,5377	250	273.23	0.0490	
	0.67838					HOMO→LUMO (92%)
		5.2655	227	235.46	0.3899	
	0.67960					HOMO→LUMO+1 (92%)
		5.5955		221.58	0.0004	
	0.70611					HOMO-1→LUMO (99%)

(nm: nanometer, Cal.: Calculated, Exp.: Experimental, eV: electron Volt, λ: Absorption wavelengths).

Table 4. Global chemical reactivity indices for the 2-ATP, 3-ATP and 4-ATP.

Parameters	2ATP [eV)]	3ATP [eV]	4-ATP [eV]
E_{HOMO}	-5.679	-5.697	-5.689
E_{LUMO}	-0.576	-0.379	-0.460
ΔE	5.121	5.243	5.229
Ionization potential ($I = - E_{HOMO}$)	5.679	5.697	5.589
Electron affinity ($A = - E_{LUMO}$)	0.576	0.379	0.460
Electronegativity ($\chi = (I+A)/2$)	3.128	3.038	3.075
Chemical potential ($\mu = -(I+A)/2$)	-3.128	-3.038	-3.075
Chemical hardness ($\eta = (I-A)/2$)	2.552	2.659	2.615
Chemical softness ($s = 1/2\eta$)	0.196	0.188	0.191
Electrophilic index ($w = \mu^2/2\ \eta$)	1.917	1.735	1.808
Maximum load transfer parameter ($\Delta N_{max} = (I+A)/(I-A)$)	1,378	1,142	1,176

HOMO energies are calculated as -5.697, -5.622, and -5.689 eV for 2-ATP, 3-ATP, 4-ATP, respectively. LUMO energies are calculated as -0.576, -0.379, and -0.460 eV, respectively. Also, the energy gap between the HOMO and LUMO orbital is determined as 5.121, 5.243, and 5.229 eV for 2-ATP, 3-ATP, 4-ATP, respectively. In the literature review, it was observed that when the HOMO-LUMO energy gap is greater than 4.5 eV, the molecule is interpreted as being chemically stable [41, 42]. The relatively high HOMO-LUMO energy gap value indicates that the investigated isomers have high chemical stability and low reactivity. In this study, it is observed that 3-ATP is the most stable isomer among the ATPs. This idea has been supported by searching the literature; the publication numbers about the adsorption of 3-ATP is the least among other adsorption of ATPs.

(a

In molecules, electrons flow from high chemical potential to low chemical potential. In our molecules, χ values are defined as 3.128, 3.038 and 3.075 eV for 2-ATP, 3-ATP and 4-ATP, respectively. From the HOMO and LUMO energies, the η values are defined as 2.552, 2.659, and 2.615 eV for 2- ATP, 3- ATP, and 4-ATP, respectively. When the electronegativity of the isomers was examined, it was calculated as 3.128, 3.038, 3.075 eV for 2-ATP, 3-ATP and 4-ATP, respectively.

NLO analysis

The first and second hyperpolarization values for molecular systems depend on the efficiency of electronic communication between donor and withdrawing groups, which play an important role in intramolecular charge transfer. For the ATPs molecules, the dipole moment (μ), the polarizabilities (α) and the first-order hyperpolarizabilities (β) at the static state were computed by using keyword polar=enonly with the B3LYP/LanL2DZ level. The quantities of μ, α and β in terms of x, y, and z components are listed in Table 5. The μ_{total}, $<\alpha>$ and β_{total} quantities were obtained via the following equations [43];

$$\mu_{total} = \left(\mu_x{}^2 + \mu_y{}^2 + \mu_z{}^2\right)^{\frac{1}{2}}$$

$$\alpha_{total} = \frac{1}{3}\left(\alpha_{xx} + \alpha_{yy} + \alpha_{zz}\right)$$

$$\beta_{total} = \sqrt{\left(\beta_{xxx} + \beta_{xyy} + \beta_{xzz}\right)^2 + \left(\beta_{yyy} + \beta_{yzz} + \beta_{yxx}\right)^2 + \left(\beta_{zzz} + \beta_{zxx} + \beta_{zyy}\right)^2}$$

Table 5. Dipole moments, static average polarizability, further extended first hyperpolarizability of 2- ATP, 3- ATP and 4- ATP.

Components	2-ATP	3-ATP	4-ATP
μ_x	-0.210	-0.915	2.201
μ_y	0.736	0.034	0.00009
μ_z	0.346	0.0002	0.450
μ_{total} (Debye)	0.841	0.979	2.247
α_{xx} (a.u.)	112.698	123.246	156.832
α_{yy} (a.u.)	92.185	94.483	80.447
α_{zz} (a.u.)	42.769	32.033	45.710
$<\alpha>$ (a.u.)	82.551	83.254	94.330
$<\alpha>$ (esu)	12.234×10^{-24}	12.338×10^{-24}	13.980×10^{-24}
β_{xxx} (a.u.)	-54.18	-227.04	-669.76
β_{xxy} (a.u.)	-89.24	259.02	0.053
β_{xyy} (a.u.)	-157.73	14.08	184.70
β_{yyy} (a.u.)	-80.71	69.76	0.63
β_{xxz} (a.u.)	15.73	0.25	21.01
β_{yyz} (a.u.)	-6.83	-0.12	13.16
β_{xzz} (a.u.)	-5.79	-31.86	5.47
β_{yzz} (a.u.)	-3.63	17.03	0.10
β_{zzz} (a.u.)	32.51	0.13	31.16
β_{total} (a.u.)	281.49	390.37	484.02
β_{total} (esu)	2.429×10^{-30}	3.369×10^{-30}	4.178×10^{-30}

(μ_x = dipole moment at x direction, μ_y = dipole moment at y direction, μ_z = dipole moment at z direction, α= dipole polarizability, $<\alpha>$ = static average dipole polarizability, β = furter extended first hyperpolarizabilities a.u. = atomic unit, for α, 1 a.u. = 0.1482×10^{-24} esu, for β, 1 a.u. = 0.008629×10^{-30} esu).

The static μ_{total}, $<\alpha>$, and β_{total} values of the 2-ATP were calculated as 0.841 Debye, 12.234×10^{-24} esu, and 2.429×10^{-30} esu, respectively. Similarly, for 3-APT, these values were calculated as 0.979 Debye, $12{,}338\times10^{-24}$ esu, $3{,}369\times10^{-30}$ esu, and for 4-ATP, these values were determined as 2.247 Debye, 13.980×10^{-24} esu, 4.178×10^{-30} esu, μ_{total}, $<\alpha>$, and β_{total}, respectively. For 4-ATP, the dipole moment value in the x axes is higher than the other axes, and at this value it is 2.247 Debye. The hyperpolarizability value of urea is used as a reference in compounds with nonlinear optical properties [44, 45]. When we survey the literature, the dipole moment (μ) and first-order hyperpolarizabilities values (β) of urea calculated by the B3LYP/LanL2DZ method are 1.3732D and 0.3782 x 10^{-30} esu, respectively [44]. When the hyperpolarizability value of ATPs are compared with urea, the hyper polarizable values of ATP isomers appear to be higher than that of urea. Since ATP isomers have a higher intramolecular charge transfer than urea, these isomers are very good candidates for nonlinear optical materials.

CONCLUSION

The vibrational frequencies of an organic molecule have got a unique spectrum for each organic compound. In this point of view, IR spectroscopy has a feature for the identification of chosen isomer set. It is explained how the geometrical differences in molecular dimensions of isomers with the same chemical formula and molecular weight affect the properties of the molecule such as characteristic wavenumbers, polarizability, electronegativity, HOMO-LUMO energies.

It was observed that vibration frequencies increased around 1200 cm^{-1} as the amine group moved away from the ring-bound S-H group in ATPs. NH_2 is attached to the ring on the C1 atom in all three isomers. However, the angle between C6-C1-C2 carbon atoms, which are in the same order in all isomers, differs in each isomer. For ATPs, it can be said that these differences are due to both the change in the place where the thiol group is attached to the phenyl ring and the distance between the amine and thiol group.

In Figure 4c, it is seen that the negative and positive charge densities are concentrated at the opposite ends of the molecule. The yellow pole with the thiol group is seen as the region where more electrons are collected, while the blue pole with the amine group shows the electron-poor region. The most striking feature of 4-ATP is the distribution of charges on a straight line and this caused the 4 ATP to look like a dipole. In Figure 5, it is sighted viewed that the images of the HOMO-LUMO energies of 4-ATP are quite symmetrical. The property of 4 ATP shows that the charge distributions are symmetrical as in a dipole. This feature indicates that the adsorption properties of 4-ATP are higher than other isomers [46]. When the study of Batz *et al.* was examined, it was observed that 4-ATP was the most concentrated in the monolayer among the other isomers.

In the literature study, it was realized that 4-ATP was used more frequently in adsorption studies than other isomers. As a result of the experimental and theoretical examination in our study, it is estimated that the symmetry, spatial positioning, and electrical charge distribution of the 4- ATPs may cause this. The information that the dipole moment is effective in facilitating the adsorption of ATPs was given in a study. There is also a study showing that 4-ATP has a high adsorption capacity in studies on corrosion [10, 47].

The relatively high HOMO-LUMO energy gap value indicates that the investigated isomers have high chemical stability and low reactivity. It means they do not show affinity to give in a chemical reaction in room condition. In this study, it is seen that 3-ATP is the most stable isomers among others. Among the isomers, the largest μ value belongs to 4-ATP and its value is 2.241 D, also dipole moment (μ_{total}), polarizability ($<\alpha>$) and hyper polarizability (β_{total}) has the biggest value for 4-ATP as can be seen in Table 5. The hyperpolarizability values of ATPs shows that ATP molecules are very good candidates for nonlinear optical materials.

REFERENCES

1. Kabel, K.I.; Zakaria, K.; Abbas, M.A.; Khamis, E.A. Assessment of corrosion inhibitive behavior of 2-aminothiophenol derivatives on carbon steel in 1 M HCl. *J. Ind. Eng. Chem.* **2015**, 23, 57–66.
2. Mohamed, T.A.; Soliman, U.A.; Hanafy, A.I.; Hassan, A.M. Conformational stability, barriers to internal rotation of 2-aminothiophenol (D0 and D3): A combined vibrational and theoretical approach. *J. Mol. Struct. THEOCHEM* **2008**, 865, 14–24.
3. Yilmaz, Y.Y.; Yalcinkaya, E.E.; Demirkol, D.O.; Timur, S. 4-Aminothiophenol-intercalated montmorillonite: Organic-inorganic hybrid material as an immobilization support for biosensors. *Sensors Actuators, B Chem.* **2020**, 307, 127665.
4. Wu, D.Y.; Zhao, L. Bin; Liu, X.M.; Huang, R.; Huang, Y.F.; Ren, B.; Tian, Z.Q. Photon-driven charge transfer and photocatalysis of *p*-aminothiophenol in metal nanogaps: A DFT study of SERS. *Chem. Commun.* **2011**, 47, 2520–2522.
5. Ferraresi-Curotto, V.; Echeverría, G.A.; Piro, O.E.; Pis-Diez, R.; González-Baró, A.C. An experimental and DFT study of a disulfide-linked Schiff base: Synthesis, characterization and crystal structure of bis (3-methoxy-salicylidene-2- aminophenyl) disulfide in its anhydrous and monohydrate forms. *Spectrochim. Acta - Part A Mol. Biomol. Spectrosc.* **2014**, 118, 279–286.
6. Maniu, D.; Chis, V.; Baia, M.; Toderas, F.; Astilean, S. Density functional theory investigation of p-aminothiophenol molecules adsorbed on gold nanoparticles. *J. Optoelectron. Adv. Mater.* **2007**, 9, 733–736.
7. Batz, V.; Schneeweiss, M.A.; Kramer, D.; Hagenström, H.; Kolb, D.M.; Mandler, D. Electrochemistry and structure of the isomers of aminothiophenol adsorbed on gold. *J. Electroanal. Chem.* **2000**, 491, 55–68.
8. Polewska, W.; Vogt, M.R.; Magnussen, O.M.; Behm, R.J. In situ STM study of Cu(II) surface structure and corrosion in pure and benzotriazole-containing sulfuric acid solution. *J. Phys. Chem. B* **1999**, 103, 10440–10451.
9. Quan, Z.; Chen, S.; Li, Y.; Cui, X. Adsorption behaviour of Schiff base and corrosion protection of resulting films to copper substrate. *Corros. Sci.* **2002**, 44, 703–715.
10. Li, J.; Zhang, M. Atomic insights into adsorption of thiophenol derivatives as corrosion inhibitors for mild steel in hydrochloric acid solution. *Mater. Res. Innov.* **2014**, 18, 38–42.
11. Karthik, N.; Asha, S.; Sethuraman, M.G. Influence of pH-sensitive 4-aminothiophenol on the copper corrosion inhibition of hybrid sol–gel monolayers. *J. Sol-Gel Sci. Technol.* **2016**, 78, 248–257.
12. Jeraldin, U.A.M.; Santhi, R.J. Isomers of poly (aminothiophenol): Chemical synthesis and corrosion inhibition of mild steel in acidic medium. *Ann. Romanian Soc. Cell Biol.* **2021**, 25, 17091–17106.
13. Jeraldin, U.A.M.; Shanthi, R.J. Synthesis, characterizations and antibacterial studies of conducting poly aminothiophenols. *Iarjset* **2018**, 5, 110–118.
14. Sorasaenee, K.; Galán-Mascarós, J.R.; Dunbar, K.R. Reactivity studies of anticancer active dirhodium complexes with 2-aminothiophenol. *Inorg. Chem.* **2002**, 41, 433–436.
15. Hutchison, J.A.; Centeno, S.P.; Odaka, H.; Fukumura, H.; Hofkens, J.; Uji-i, H. Subdiffraction limited, remote excitation of surface enhanced Raman scattering. *Nano Lett.* **2009**, 9, 995–1001.
16. Villarreal, E.; Li, G.G.; Zhang, Q.; Fu, X.; Wang, H. Nanoscale surface curvature effects on ligand-nanoparticle interactions: A Plasmon-enhanced spectroscopic study of thiolated ligand adsorption, desorption, and exchange on gold nanoparticles. *Nano Lett.* **2017**, 17, 4443–4452.
17. Ward, D.R.; Halas, N.J.; Ciszek, J.W.; Tour, J.M.; Wu, Y.; Nordlander, P.; Natelson, D. Simultaneous measurements of electronic conduction and raman response in molecular junctions. *Nano Lett.* **2008**, 8, 919–924.
18. Sun, M.; Xu, H. Direct visualization of the chemical mechanism in SERRS of 4-

aminothiophenol/metal complexes and metal/4-aminothiophenol/metal junctions. *ChemPhysChem* **2009**, 10, 392–399.
19. Jiang, R.; Zhang, M.; Qian, S.L.; Yan, F.; Pei, L.Q.; Jin, S.; Zhao, L. Bin; Wu, D.Y.; Tian, Z. Q. Photoinduced surface catalytic coupling reactions of aminothiophenol derivatives investigated by SERS and DFT. *J. Phys. Chem. C* **2016**, 120, 16427–16436.
20. Rosario-Castro, B.I.; Fachini, E.R.; Hernández, J.; Pérez-Davis, M.E.; Cabrera, C.R. Electrochemical and surface characterization of 4-aminothiophenol adsorption at polycrystalline platinum electrodes. *Langmuir* **2006**, 22, 6102–6108.
21. Frisch M.J.; Trucks, G.W.; Schlegel, H.B.; Scuseria, G.E.; Robb, M.A.; Cheeseman, J.R.; Scalmani, G.; Barone, V.; Mennucci, B.; Petersson, G.A.; Nakatsuji, H.; Caricato, M.; Li, X., Hratchian, H.P.; Izmaylov, A.F.; Bloino, J.; Zheng, G.; Sonnenberg, J.L.; Hada, M.; Ehara, M., Toyota, K.; Fukuda, R.; Hasegawa, J.; Ishida, M.; Nakajima, T.; Honda, Y.; Kitao, O.; Nakai, H.; Vreven, T.; Montgomery J.A.; Peralta, J.E.; Ogliaro, F.; Bearpark, M.; Heyd, J.J.; Brothers, E.; Kudin, K.N.; Staroverov, V.N.; Kobayashi, R.; Normand, J.; Raghavachari, K.; Rendell, A.; Burant, J.C.; Iyengar, S.S.; Tomasi, J.; Cossi, M.; Rega, N; Millam, J.M.; Klene, M.; Knox, J.E.; Cross, J.B.; Bakken, V.; Adamo, C.; Jaramillo, J.; Gomperts, R.; Stratmann, R.E.; Yazyev, O.; Austin, A.J.; Cammi, R.; Pomelli, C.; Ochterski, J.W.; Martin, R.L.; Morokuma, K.; Zakrzewski, V.G.; Voth, G.A.; Salvador, P.; Dannenberg, J.J.; Dapprich, S.; Daniels, A.D.; Farkas, Ö.; Foresman, J.B.; Ortiz, J.V.; Cioslowski, J.; Fox, D.J. Gaussian 09, Gaussian, Inc.: Wallingford; **2003**.
22. Dennington, R.D.; Keith, T.A.; Millam, J.M. Gauss Wiev 5.0: Wallingford; **2009**.
23. Jamroz, M.H. *Vibrational Energy Distribution Analysis VEDA 4.0*, Drug Institute: Warsaw, Poland; **2004**.
24. Badawi, H.M.; Förner, W.; Ali, S.A. A comparative study of the infrared and raman spectra of aniline and *o*-, *m*-, *p*-phenylenediamine isomers. *Spectrochim. Acta - Part A Mol. Biomol. Spectrosc.* **2013**, 112, 388–396.
25. Liang, X.; Xu, Y.; Sun, G.; Wang, L.; Sun, Y.; Qin, X. Preparation, characterization of thiol-functionalized silica and application for sorption of Pb^{2+} and Cd^{2+}. *Colloids Surfaces A Physicochem. Eng. Asp.* **2009**, 349, 61–68.
26. Sägmüller, B.; Freunscht, P.; Schneider, S. The assignment of the vibrations of substituted mercaptotetrazoles based on quantum chemical calculations. *J. Mol. Struct.* **1999**, 482–483, 231–235.
27. Bazylewski, P.; Divigalpitiya, R.; Fanchini, G. In situ Raman spectroscopy distinguishes between reversible and irreversible thiol modifications in L-cysteine. *RSC Adv.* **2017**, 7, 2964–2970.
28. Merrick, J.P.; Moran, D.; Radom, L. An evaluation of harmonic vibrational frequency scale factors. *J. Phys. Chem. A* **2007**, 111, 11683–11700.
29. Balachandran, V.; Lalitha, S.; Rajeswari, S. Density functional theory, comparative vibrational spectroscopic studies, NBO, HOMO-LUMO analyses and thermodynamic functions of N-(bromomethyl) phthalimide and N-(chloromethyl)phthalimide. *Spectrochim. Acta - Part A Mol. Biomol. Spectrosc.* **2012**, 91, 146–157.
30. Hu, H.; Yang, X.; Zhai, F.; Hu, D.; Liu, R.; Liu, K.; Sun, Z.; Dai, Q. Far-field nanoscale infrared spectroscopy of vibrational fingerprints of molecules with graphene plasmons. *Nat. Commun.* **2016**, 7, 1–8. https://doi.org/10.1038/ncomms12334.
31. Almutlaq, N.; Al-Hossainy, A.F.; Zoromba, M.S. Combined experimental and theoretical study, characterization, and nonlinear optical properties of doped-poly (p-nitroaniline -Co-*o*-aminophenol) thin films. *J. Mol. Struct.* **2021**, 1227, 129712.
32. Slimane, A.B.; Al-Hossainy, A.F.; Zoromba, M.S. Synthesis and optoelectronic properties of conductive nanostructured poly(aniline-Co-o-aminophenol) thin film. *J. Mater. Sci.: Mater. Electron.* **2018**, 8431–8445.
33. Madzharova, F.; Heiner, Z.; Kneipp, J. Surface-enhanced hyper raman spectra of aromatic thiols on gold and silver nanoparticles. *J. Phys. Chem. C* **2020**, 124, 6233–6241.

34. Govindarajan, M.; Ganasan, K.; Periandy, S.; Mohan, S. DFT (LSDA, B3LYP and B3PW91) comparative vibrational spectroscopic analysis of α-acetonaphthone. *Spectrochim. Acta - Part A Mol. Biomol. Spectrosc.* **2010**, 76, 12–21.
35. Minaeva, V.; Minaev, B.; Panchenko, A.; Pasychnik, V. Computational study of IR, Raman, and NMR spectra of 4-methylmethcathinone drug. *J. Mol. Model.* **2021**, 27. https://doi.org/10.1007/s00894-020-04658-0.
36. Demircioɨlu, Z.; Kaştaş, Ç.A.; Büyükgüngör, O. Theoretical analysis (NBO, NPA, Mulliken population method) and molecular orbital studies (hardness, chemical potential, electrophilicity and Fukui function analysis) of (e)-2-((4-hydroxy-2-methylphenylimino)methyl)-3-methoxyphenol. *J. Mol. Struct.* **2015**, 1091, 183–195.
37. Alam, M.; Park, S. Molecular structure, spectral studies, NBO, HOMO–LUMO profile, MEP and Mulliken analysis of 3β,6β-dichloro-5α-hydroxy-5α–cholestane. *J. Mol. Struct.* **2018**, 1159, 33–45.
38. Boxi, S.; Jana, D.; Ghorai, B.K. Synthesis and optical properties of bipolar quinoxaline-triphenylamine based stilbene compounds. *Opt. Mater. X* **2019**, 1, 100013.
39. Franco-Pérez, M.; Gázquez, J.L. Electronegativities of Pauling and Mulliken in Density functional theory. *J. Phys. Chem. A* **2019**, 123, 10065–10071.
40. Kutlu, E.; Mehmet, F.; Kismali, G.; Kaya, N.; Kılıç, D.; Ihsan, A.; Esra, R. Pyridine derivative platinum complexes : Synthesis, molecular structure, DFT and initial anticancer activity studies. *J. Mol. Struct.* **2021**, 1234, 130191.
41. Sadgir, N.V.; Dhonnar, S.L.; Jagdale, B.S.; Sawant, A.B. Synthesis, spectroscopic characterization, XRD crystal structure, DFT and antimicrobial study of (2E)-3-(2,6-dichlorophenyl)-1-(4-methoxyphenyl)-prop-2-en-1-one. *SN Appl. Sci.* **2020**, 2, 1–12.
42. Rocha, M.; Santo, A.Di; Altabef, A.Ben; Gil, D.M. Intermolecular interactions, spectroscopic and theoretical investigation of 4-aminoacetophenone. *Int. J. Adv. Chem.* **2019**, 7, 1–12.
43. Kecel-Gunduz, S.; Bicak, B.; Celik, S.; Akyuz, S.; Ozel, A.E. Structural and spectroscopic investigation on antioxidant dipeptide, l-methionyl-l-serine: A combined experimental and DFT study. *J. Mol. Struct.* **2017**, 1137, 756–770.
44. Anbarasan, R.; Eniya, P.; Kalyana Sundar, J. Experimental and quantum chemical investigation on piperazinium hexachloro stannous trihydrate single crystal for second harmonic generation applications. *J. Electron. Mater.* **2019**, 48, 7686–7695.
45. Kanagathara, N.; Usha, R.; Natarajan, V.; Marchewka, M.K. Molecular geometry, vibrational, NBO, HOMO–LUMO, first order hyper polarizability and electrostatic potential studies on anilinium hydrogen oxalate hemihydrate–an organic crystalline salt. *Inorg. Nano-Metal Chem.* **2021**, 0, 1–8. https://doi.org/10.1080/24701556.2021.1891103.
46. Ma, Y.; Nie, B. Unraveling a self-assembling mechanism of isomeric aminothiophenol on Ag dendrite by correlated SERS and matrix-free LDI-MS. *Anal. Bioanal. Chem.* **2019**, 411, 8081–8089.
47. Yildiz, R.; Dogru Mert, B. Theoretical and experimental investigations on corrosion control of mild steel in hydrochloric acid solution by 4-aminothiophenol. *Anti-Corrosion Methods Mater.* **2019**, 66, 127–137.